A New Induction Motor *V/f* Control Method Capable of High-Performance Regulation at Low Speeds

Alfredo Muñoz-García, Thomas A. Lipo, *Fellow, IEEE*, and Donald W. Novotny, *Fellow, IEEE*

***Abstract*— A novel open-loop speed control method for induction motors that provides high output torque and nearly zero steady-state speed error at any frequency is presented. The control scheme is based on the popular constant volts per hertz (V/f) method using low-cost open-loop current sensors. Only stator current measurements are needed to compensate for both stator resistance drop and slip frequency. The scheme proposed fully compensates for the current–resistance (*IR*) voltage drop by vectorially modifying the stator voltage and keeping the magnitude of the stator flux constant, regardless of changes in frequency or load. A novel slip frequency compensation, based on a nonlinear torque–speed estimate, is also introduced. This method reduces the steady-state speed error to almost zero. It is also shown that a linear torque–speed approximation is a special case of the nonlinear estimate and that it leads to large speed errors for loads greater than rated. It is shown that, by using the proposed method, the speed can be accurately controlled down to, at least, 1.2 Hz with load torques of more than 150% of rated value. Since the only machine parameter required, the stator resistance, is automatically measured at startup time, using the same pulsewidth modulated voltage-source inverter without additional hardware, the proposed drive also exhibits self-commissioning capability.**

***Index Terms*—Constant volts per hertz, induction machine, low speed, slip compensation.**

I. Introduction

THE operation of induction motors in the so-called constant volts per hertz (V/f) mode has been known for many decades, and its principle is well understood [1], [7]. With the introduction of solid-state inverters, the constant V/f control became popular [2]–[4], and the great majority of variable-speed drives in operation today are of this type [5]. However, since the introduction of vector control theory by Blaschke [6], almost all research has been concentrated in this area, and little has been published about constant V/f operation. Its practical application at low frequency is still challenging, due to the influence of the stator resistance and the necessary rotor slip to produce torque. In addition, the nonlinear behavior of the modern pulsewidth modulated voltage-source inverter (PWM-VSI) in the low voltage range [8]–[10] makes it difficult to use constant V/f drives at frequencies below 3 Hz [11].

The simplest stator resistance compensation method consists of boosting the stator voltage by the magnitude of the current–resistance (*IR*) drop [12]. Improved techniques using the in-phase component of the stator current and a compensation proportional to a slip signal have also been proposed [7]. A vector compensation was proposed in [13], but it required both voltage and current sensors and accurate knowledge of machine inductances. More recently, a scalar control scheme was proposed [14]. In this scheme, the flux magnitude is derived from the current estimation. In [15], using the dc-link voltage and current, both flux and torque loops are introduced. Its use at low frequency is limited by the flux estimation. Also, the slip compensation was based on a linear torque–speed assumption which led to large steady-state errors in speed for high load torques. A linearized frequency compensation control based on an "ideal induction motor" was proposed in [16].

In this paper, a new stator resistance and frequency compensation technique requiring minimum knowledge of the motor's parameters is presented. The only measured quantity is the stator current. The stator resistance voltage drop is fully compensated for by vectorially adding it to the commanded voltage using both in-phase and quadrature components of the stator current. The frequency compensation is based on an estimation of the airgap power and a nonlinear relationship between slip frequency and airgap power. This method predicts the correct slip frequency for any load at any frequency. The proposed control scheme requires only nameplate data, the stator resistance value, and a reasonable estimation of the breakdown torque. The proposed method is validated by simulation and experimental results. It is shown that large torques are obtainable, even in the low speed range, with almost no steady-state error in speed.

II. Stator Resistance Compensation

The stator resistance compensation is based on keeping the stator flux-linkage magnitude constant and equal to its rated value. From the phasor diagram shown in Fig. 1, it is easy to show that the magnitude of E_m is

$$E_m^2 = (V_s)^2 + (I_s r_s)^2 - 2V_s(I_s r_s)\cos\phi. \qquad (1)$$

Paper IPCSD 98–14, presented at the 1997 Industry Applications Society Annual Meeting, New Orleans, LA, October 5–9, and approved for publication in the IEEE TRANSACTIONS ON INDUSTRY APPLICATIONS by the Industrial Drives Committee of the IEEE Industry Applications Society. This work was supported in part by the Wisconsin Electric Machines and Power Electronics Consortium (WEMPEC). Manuscript released for publication February 25, 1998.

A. Muñoz-García is with the Department of Electrical and Computer Engineering, University of Wisconsin, Madison, WI 53706-1691 USA, on leave from the Technical University Santa Maria, Valparaíso, Chile.

T. A. Lipo and D. W. Novotny are with the Department of Electrical and Computer Engineering, University of Wisconsin, Madison, WI 53706-1691 USA.

Publisher Item Identifier S 0093-9994(98)04920-2.

0093–9994/98$10.00 © 1998 IEEE

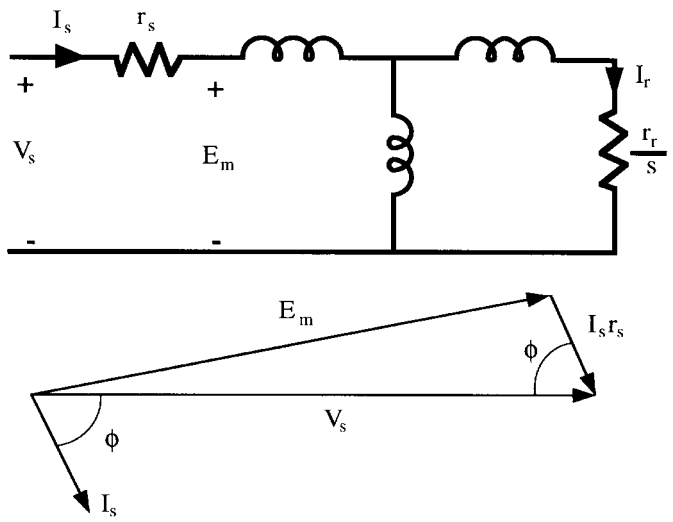

Fig. 1. Induction motor steady-state equivalent circuit and phasor diagram.

Defining V_{so} as the magnitude of E_m at rated frequency f_R, at any frequency f_e^*, the required value of E_m to accomplish true constant V/f is given by $V_{so}(f_e^*/f_R)$.

Substituting this quantity into (1) yields

$$V_s = I_s r_s \cos\phi + \sqrt{\left(\frac{V_{so} f_e^*}{f_R}\right)^2 - (I_s r_s)^2 (\sin\phi)^2} \qquad (2)$$

where V_{so} is a constant defined by rated conditions, and the subscript R indicates rated values.

To implement (2), the rms value of the stator current I_s, $\cos(\phi)$, and $\sin(\phi)$ are needed. Assuming a set of balanced sinusoidal currents, the rms value, in terms of instantaneous quantities, can be written as

$$I_s = \sqrt{\frac{2}{3}} \sqrt{i_{as}(i_{as} + i_{cs}) + i_{cs}^2}. \qquad (3)$$

The terms $\cos(\phi)$ and $\sin(\phi)$ are obtained by using a transformation similar to what is known as the complex vector form of real variables [17]. Defining the complex quantity

$$\underline{i}_s = i_{as} + \underline{a}^2 i_{bs} + \underline{a} i_{cs} \qquad (4)$$

where $\underline{a}$ is the complex number $e^{j(2\pi/3)}$; substituting the currents and using a synchronous reference frame yields

$$\underline{i}_s^e = \frac{3\hat{I}}{2} e^{j\phi} = \frac{3}{\sqrt{2}} I_s(\cos(\phi) + j\sin(\phi)) \qquad (5)$$

where $\hat{I}$ is the peak current and ϕ the phase angle. Because of the trigonometric relation between sine and cosine and the structure of (2), only the real part of (5) is required, therefore, the actual implementation does not use complex variables and (5) can be simplified to

$$\mathrm{Re}\{\underline{i}_s^e\} = I_{s(\mathrm{Re})} = \sqrt{3}\left\{ i_{as} \cos\left(\omega t - \frac{\pi}{6}\right) - i_{cs} \sin(\omega t) \right\} \qquad (6)$$

where $\mathrm{Re}\{\underline{i}_s^e\}$ has been replaced by the symbol $I_{s(\mathrm{Re})}$ to stress that only real quantities are used.

Although, by definition, the rms current and the power factor are steady-state quantities, the use of (3), (5), and (6) yields instantaneous measurements of both of them. This is a very important factor, since it gives continuous measurements that can be used for feedback purposes, allowing for better dynamics in the control. An alternate form to obtain the power factor is to measure the time delay between the zero crossings of the current and the voltage. This method, however, gives poor results for several reasons; first, the measured current contains high-frequency noise that makes it difficult to identify the exact point of zero crossing, and second, the power factor measurement can only be updated, at most, every 1/6 of a cycle. These problems are eliminated by using (3), (5), and (6). The final expression for the required stator voltage, including only instantaneously measured and commanded quantities, is

$$V_s = \frac{\sqrt{2}}{3} I_{s(\mathrm{Re})} \cdot r_s + \sqrt{\left(\frac{V_{so} f_e^*}{f_R}\right)^2 + \frac{2}{9}(I_{s(\mathrm{Re})} \cdot r_s)^2 - (I_s r_s)^2}. \qquad (7)$$

Equation (7) corresponds to a vector compensation of the *IR* drop. Given the inherently positive feedback characteristic of the *IR* boost algorithm, it is necessary to stabilize the system by introducing a first-order lag in the feedback loop (low-pass filter). Since (7) contains both the *IR* boost and the base V/f ratio, we only need to apply the lag to the boost component of the algorithm; this is shown schematically in Fig. 2.

III. Slip Frequency Compensation

In order to produce torque, an induction motor needs to develop slip. This means that the rotor only runs at synchronous speed at no load, and, for any other condition, the mechanical speed is reduced by the slip. At rated frequency, the slip is usually around 3%, and its effect can be ignored. For variable-frequency operation, however, the slip s for constant torque varies inversely proportional to the frequency (note that the product sf remains constant) and, as the frequency decreases, the slip becomes larger, and it can no longer be ignored. At sufficiently low frequencies, this effect becomes so important that if not adequately compensated for, the motor will not be able to supply the load torque and will stall.

The compensation technique used here is explained with the help of Fig. 3. Given the torque–speed curve defined by the solid line and assuming a load torque T_L, the motor will develop a slip proportional to the length AB. If the stator frequency is boosted in such a way that a new torque–speed curve, as defined by the dashed line, is obtained, then, for the same load torque, the motor will run at ω_o, which corresponds to the original synchronous speed. By continuously adjusting the stator frequency, the mechanical speed can be maintained constant for any load.

In order to implement this scheme, it is necessary to know the relationship between torque and slip (this is the length AB). This is normally done by assuming a linear relationship between torque and slip. Although this technique gives good results for high speeds, its usefulness at low frequency and large torques is limited, due to the large errors introduced

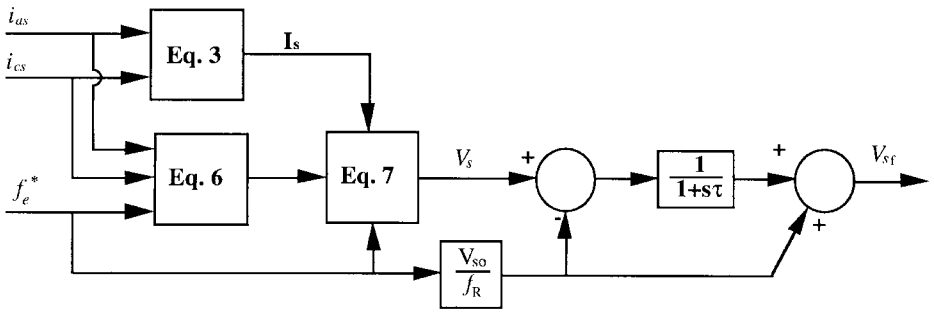

Fig. 2. *IR* compensation including first-order lag.

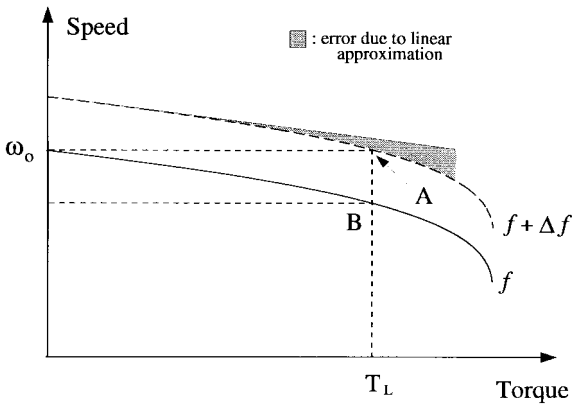

Fig. 3. Slip compensation method. The gray area shows the error introduced by a linear compensation.

by the linear approximation. The slip compensation proposed in this paper is based on the actual nonlinear torque–speed characteristic of the machine.

For typical NEMA-B design induction motors operating at rated frequency, the stator resistance is much smaller than the total leakage reactance, and the electromagnetic torque is known to be [1]

$$T_L = \frac{2T_{bd}}{\frac{s}{s_{bd}} + \frac{s_{bd}}{s}} \tag{9}$$

where T_{bd} is the breakdown torque and s_{bd} the slip at which it occurs. As the frequency is reduced, the total leakage reactance becomes smaller, and the stator resistance can no longer be ignored. However, since this effect is compensated for by the closed loop introduced in the previous section, (9) is valid for all speeds. In particular, for rated conditions and defining $T_{bd} = K_o T_R$, where T_R is the rated torque, (9) yields

$$\frac{s_{bd}}{s_R} = K = K_o + \sqrt{K_o^2 - 1} \tag{10}$$

which is the breakdown slip in per unit of the rated slip. Substituting (10) into (9) and solving for the slip yields

$$s = \frac{KK_oT_Rs_R}{T_L}\left[1 - \sqrt{1 - \left(\frac{T_L}{K_oT_R}\right)^2}\right]. \tag{11}$$

Equation (11) is the slip required to produce the electromagnetic torque T_L. To completely solve for the slip frequency, we need to eliminate the load torque from (11). This is done by using an alternate form of the electromagnetic torque [17]

$$T_L = \left(\frac{p}{4\pi}\right)\frac{P_{\text{gap}}}{f_m^* + f_{\text{slip}}} \tag{12}$$

where p is the number of poles, P_{gap} is the power transferred across the airgap, f_{slip} is the slip frequency, and f_m^* is the mechanical commanded frequency. Substituting (12) into (11) and solving for the slip frequency yields

$$f_{\text{slip}} = \frac{1}{2 - A \cdot P_{\text{gap}}} \cdot \left(\sqrt{(f_m^*)^2 + \frac{K \cdot s_{\text{lin}}}{2K_o}P_{\text{gap}} - B \cdot P_{\text{gap}}^2} - f_m^*\right) \tag{13a}$$

if $A \cdot P_{\text{gap}} \neq 2$, and

$$f_{\text{slip}} = \frac{B}{A \cdot f_m^*} \quad \text{if } A \cdot P_{\text{gap}} = 2 \tag{13b}$$

where the constants A and B are defined as

$$A = \left(\frac{p}{4\pi KK_oT_Rs_Rf_R}\right), \qquad B = \left(\frac{p}{4\pi K_oT_R}\right)^2$$

and

$$s_{\text{lin}} = \left(\frac{p}{\pi}\right)\frac{s_Rf_R}{T_R} = \text{constant}.$$

The substitution of (12) into (11) and subsequent solution for the slip frequency yields a quadratic equation, the solution of which is given by (13a). For the particular case when the product $AP_{\text{gap}} = 2$, however, the coefficient of the quadratic term is zero and the solution corresponds to (13b). This does not introduce a discontinuity in the slip frequency, but it is just a consequence of the manipulation of the equations. The details of the derivation are omitted for the sake of space.

In contrast to (13), the widely used linear torque–speed approximation [15], [16], using the same notation of (13), yields a simpler expression given by

$$f_{\text{slip}} \approx \tfrac{1}{2}\left(\sqrt{(f_m^*)^2 + s_{\text{lin}}P_{\text{gap}}} - f_m^*\right). \tag{14}$$

Notice that, when K_o is large A and B become small, and (13) converges to (14). The physical meaning of this is that the linear approximation assumes a machine with an infinite breakdown torque. Although the exact value of K_o

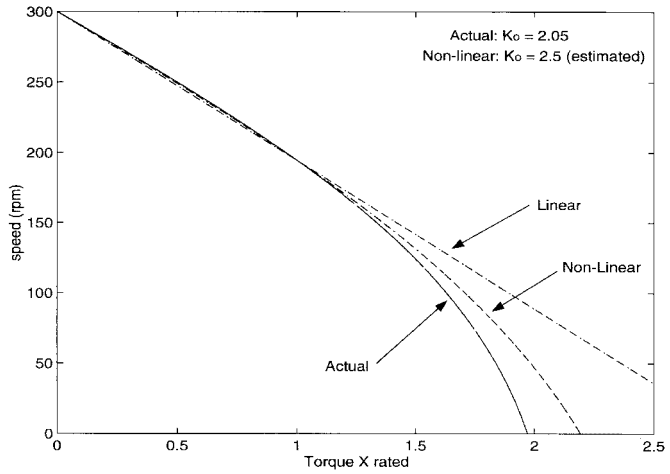

Fig. 4. Torque–speed curve. Linear and nonlinear torque approximations (the solid line corresponds to the actual curve).

is not generally known, it certainly is a finite quantity and, for a typical NEMA B design, its value lies between 1.5–3. Hence, the use of (13) provides a huge improvement over the linear approximation. To illustrate the difference between (13) and (14), actual and estimated torque–speed curves using both schemes are presented in Fig. 4. A 20% error on K_o has been intentionally added to the nonlinear prediction. If the correct value of K_o were to be used, there would be no error, and the nonlinear prediction would lie on top of the actual curve.

As shown in Fig. 4, the error introduced by the linear approximation is reasonably small for torques less than rated value, but the error increases very rapidly for larger torques. On the other hand, the nonlinear approach gives much smaller errors, even using an incorrect estimate of the breakdown torque. The difference becomes even more important at torques larger than rated value.

IV. Airgap Power Measurement

Given the importance of the airgap power in the implementation of the frequency compensation algorithm, the measurement procedure will be discussed here in some detail. This power is defined by

$$P_{\text{gap}} = 3V_sI_sPF - 3I_s^2r_s - P_{\text{core}} \tag{15}$$

where PF is the power factor and P_{core} the total core losses.

If the commanded and terminal voltages are equal, the first term of (15) is obtained using (3) and (6). The second term is readily available from the current measurement (3). The last term needs some additional consideration. In general, the core loss under variable-frequency operation is difficult to obtain, but it can be approximated from the knowledge of rated values and constant flux density operation. The core loss at rated conditions is

$$P_{\text{core}_R} = P_{\text{in}_R}(1-\eta_R) - 3I_{s_R}^2r_s - 3I_{r_R}^2r_r \tag{16}$$

where η_R is the rated efficiency (nameplate data). It is not difficult to show that for rated load

$$3I_{r_R}^2r_r = \frac{s_R}{1-s_R}P_{\text{out}_R} \tag{17}$$

TABLE I
Induction Machine Data

3 Hp	$r_s = 0.89\ \Omega$	(1)
230 V	$r_r = 0.73\ \Omega$	(2)
9 A	$L_s = 0.065$ H	(2)
60 Hz	$L_r = 0.065$ H	(2)
1740 rpm	$L_m = 0.062$ H	(3)

(1): DC measurement; (2): Locked rotor test; (3): No-load test

and substituting (17) into (16) yields

$$P_{\text{core}_R} = P_{\text{in}_R}\left(1 - \frac{\eta_R}{1-s_R}\right) - 3I_{S_R}^2r_s \tag{18}$$

where s_R is the rated slip and P_{in_R} is the total input power at rated conditions. It is common practice to separate the core loss into hysteresis and eddy-current components. This separation takes the form [18]

$$P_{\text{core}_R} = K_hB_R^2f_R + K_eB_R^2f_R^2 \tag{19}$$

where K_h and K_e depend on the core type, B_R is the rated flux density, and f_R the rated frequency.

For constant flux operation (ideal V/f), these losses only vary with frequency. Assuming that at rated conditions both components are equal, after some manipulation, the total core loss at any frequency can be written in terms of its rated value as

$$P_{\text{core}} = \frac{1}{2}\left(\frac{1+s}{1+s_R}\left(\frac{f_e^*}{f_R}\right) + \frac{1+s^2}{1+s_R^2}\left(\frac{f_e^*}{f_R}\right)^2\right)P_{\text{core}_R}. \tag{20}$$

Substituting (20) into (15) gives the air-gap power as a function of commanded frequency and measured variables. The slip measurement required in (20) is obtained from (13).

V. Simulation and Experimental Results

The proposed control scheme was first simulated and then implemented in the laboratory. The simulations were carried out using MATLAB and ACSL.

To validate the proposed control method, the algorithms were implemented using a commercial inverter and a standard 3-hp NEMA-B machine, the parameters of which are listed in Table I. The control software was developed on a Motorola 56000 digital signal processor (DSP) system, which replaced the microprocessor in the inverter. The only machine data required by the software are the rated voltage and current, number of poles, horsepower rating, and nominal frequency.

The real-time control and measurement program was written in Assembly language. The sampling time was chosen as 135 μs, and the total control program execution time is approximately 100 μs. A complete block diagram of the proposed V/f algorithm is shown in Fig. 5, while the experimental setup is shown in Fig. 6.

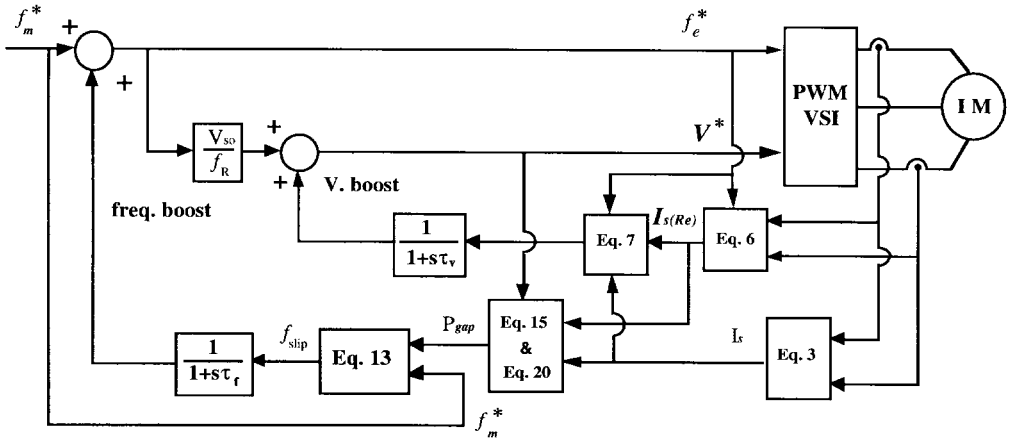

Fig. 5. Advanced induction motor V/f control, including voltage boost and slip frequency compensation loops.

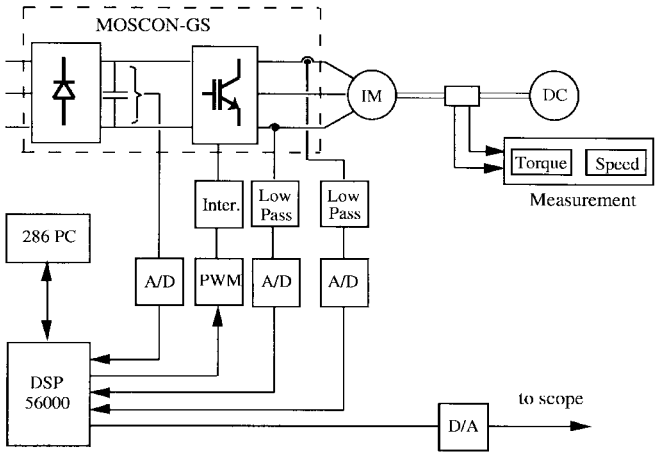

Fig. 6. Experimental setup.

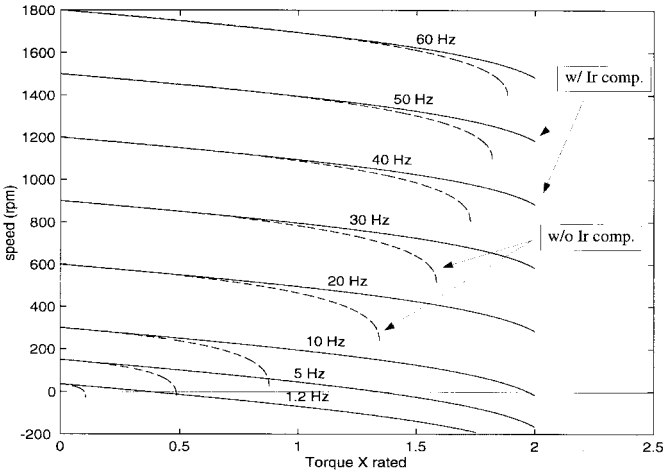

Fig. 7. *IR* compensation, steady-state model simulation results. Solid line: including *IR* compensation algorithm; dashed line: without *IR* compensation.

A. IR Compensation

The effectiveness of the stator resistance compensation algorithm was evaluated by measuring the resultant torque–speed characteristics at different frequencies and verifying that the slope of the curves remains constant.

The simulated results are shown in Fig. 7, and the experimental measurements are presented in Fig. 8. An excellent response in both cases is clearly seen. The lower limit on the frequency used in the experimental part is due to the machine stalling at lower frequencies.

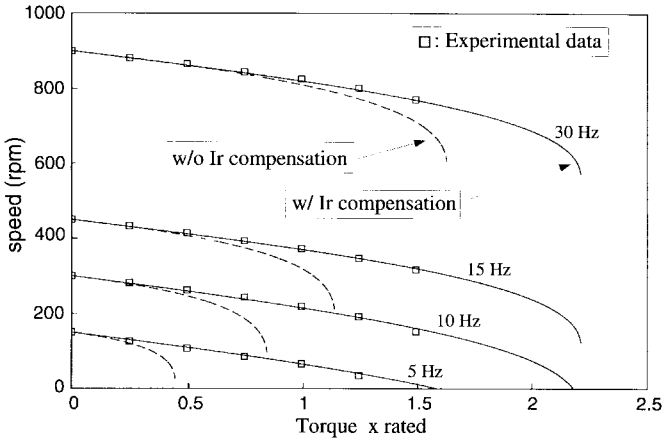

Fig. 8. Speed response, including the *IR* compensation algorithm. Experimental and simulation results are overlapped.

B. Slip Compensation

Both the linear and nonlinear slip compensation techniques were simulated and tested in the laboratory. The speed range used in the experimental part was from 1.2 Hz (36 r/min) to 60 Hz (1800 r/min) for loads up to 150% of rated value. The lower limit on the frequency was primarily imposed by the capability to accurately synthesize the commanded voltage with the PWM inverter.

1) Steady-State Response: The simulation results are shown in Fig. 9. As predicted, the linear slip compensation yields large speed errors for torques beyond rated value. For the nonlinear method, a 20% error on the estimated breakdown torque has been intentionally introduced. It can be seen that the technique is very insensitive to errors in this parameter. Fig. 10 shows the measured torque–speed curves using the nonlinear slip compensation. The measured magnitude of the stator currents for the same conditions are presented in Fig. 11.

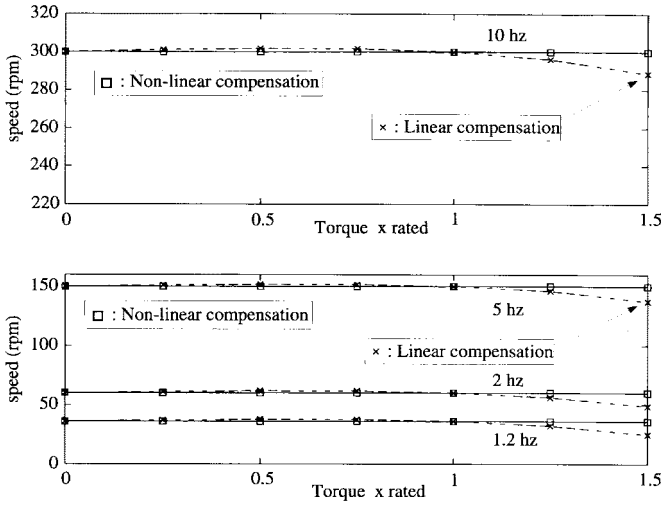

Fig. 9. Speed response, including slip compensation. Simulation results. Solid line: nonlinear method; dashed line: linear approximation.

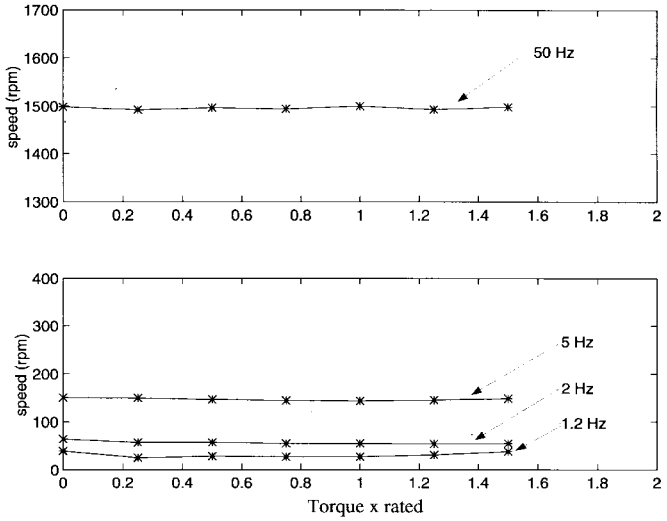

Fig. 10. Steady-state speed response, including *IR* compensation and slip compensation. Experimental results.

To illustrate the importance of the slip compensation method, measurements at 10 Hz are presented in Table II. As shown, the nonlinear method gives nearly zero speed error, while the linear approximation yields almost a 6% error.

2) Dynamic Behavior: Usually, a constant V/f drive is not used for high-performance applications, and its dynamic response is not of primary concern; however, all drives should exhibit a reasonable dynamic response and avoid instability problems.

Simulation results showing the response to a rated torque change at 1.2 Hz and to a ramp speed command are presented in Figs. 12 and 13. In the first case, the motor initially stalls after the load is applied, and after 1 s, the drive recovers and reaches the final speed with zero steady-state error. The response to a ramp command shows a good dynamic behavior.

Fig. 14 shows the experimental response to a rated torque at 7-Hz commanded frequency, and Fig. 15 shows the response at 2 Hz. In both cases, the dynamic response is reasonably

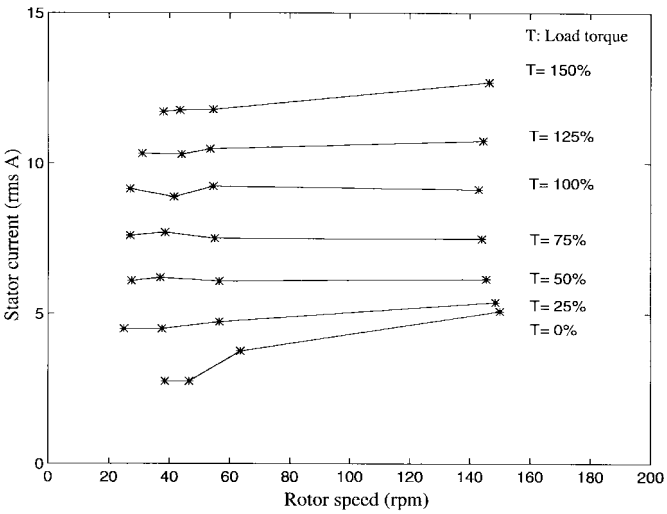

Fig. 11. Steady-state stator current response, including *IR* and slip compensation. Experimental results.

TABLE II
MEASURED SPEED RESPONSE AT 10 Hz

Torque	No compensation	Linear compensation	Non-linear compensation
(%)	speed (rpm)	speed (rpm)	speed (rpm)
100	235	290	298
150	173	283	299

fast and very stable. Finally, Fig. 16 shows the acceleration from 0 to 30 Hz.

The experimental results show the excellent response achieved with the proposed control method, even at extremely low frequencies. Also, the dynamic response indicates very good behavior over the whole frequency range.

VI. STATOR RESISTANCE MEASUREMENT

As it was pointed out in Section I, the only machine parameter required to implement the control algorithm is the stator resistance. This parameter is measured during startup using the same PWM-VSI inverter.

The stator resistance is measured by applying a dc voltage between two of the stator phases and leaving the third one disconnected. The dc voltage is synthesized using the same PWM inverter and commanding a constant voltage. By commanding $+V_{\text{test}}$ to one phase and $-V_{\text{test}}$ to another, the line–line voltage contains a dc component $(2 * V_{\text{test}})$ plus high-frequency components starting at twice the switching frequency.

The measurement procedure is as follows. After applying the test voltage, the measurement algorithm waits for approximately 0.6 s before starting the current measurement routine; this is done to avoid the influence of transients during the measurement. After the waiting period, the current is sampled 4096 times over a time interval of approximately 0.5 s, and the average value is computed. The stator resistance is obtained by dividing the applied voltage by the current.

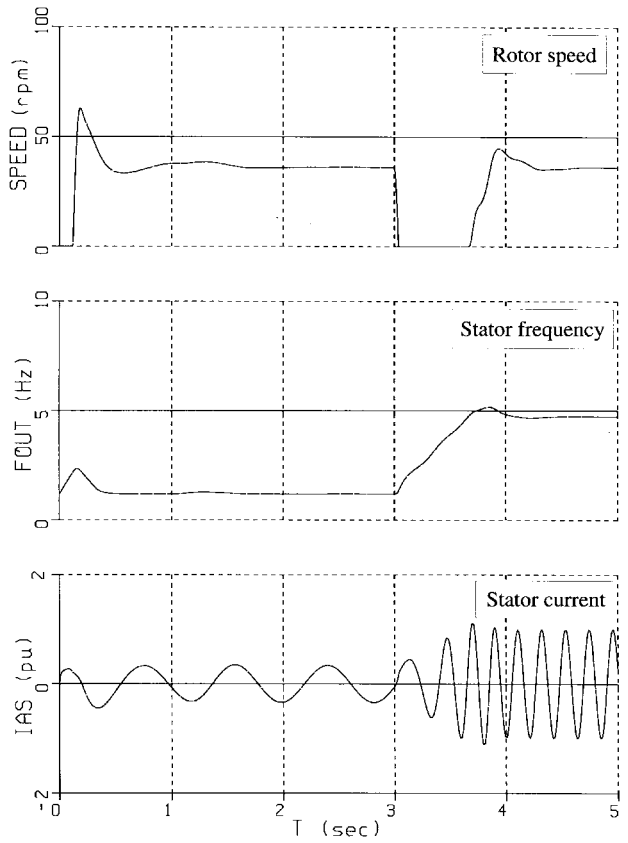

Fig. 12. Simulated no-load start at 1.2 Hz commanded frequency. Full load applied at $t = 3$ s. A 10% breakaway torque at zero speed is included. Top trace: rotor speed in revolutions per minute; middle trace: stator frequency in hertz; bottom trace: instantaneous phase stator current in per unit of rated current.

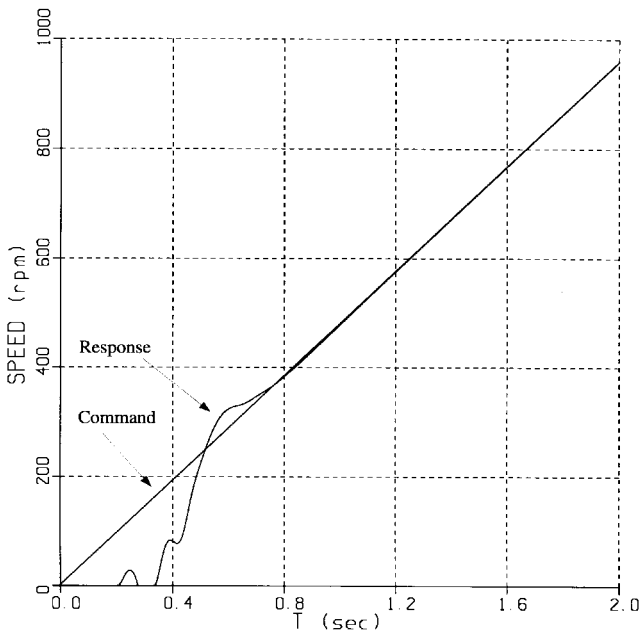

Fig. 13. Simulated response to a ramp command with full load.

This procedure yields very good accuracy, with errors less than 2%. The accuracy of the method is basically defined by the accuracy of the current sensor and the quality of the synthesized output voltage. In this case, the accuracy of the current sensors is fixed at 1%. The accuracy of the output voltage is guaranteed by using a dc-link voltage measurement and adjusting the value of V_{test} accordingly. The repeatability of the test is excellent, yielding results that are consistent to a fraction of a percent.

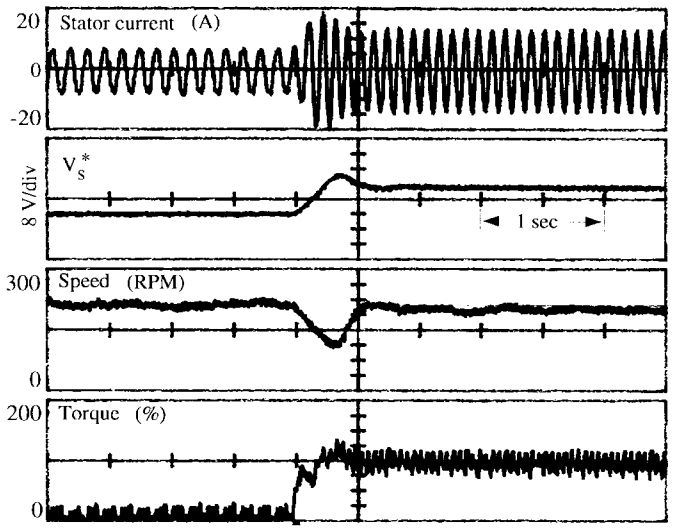

Fig. 14. Experimental rated torque change. Commanded frequency 7 Hz. Speed error 0.27%. From top: stator current, commanded voltage (magnitude), speed, and torque.

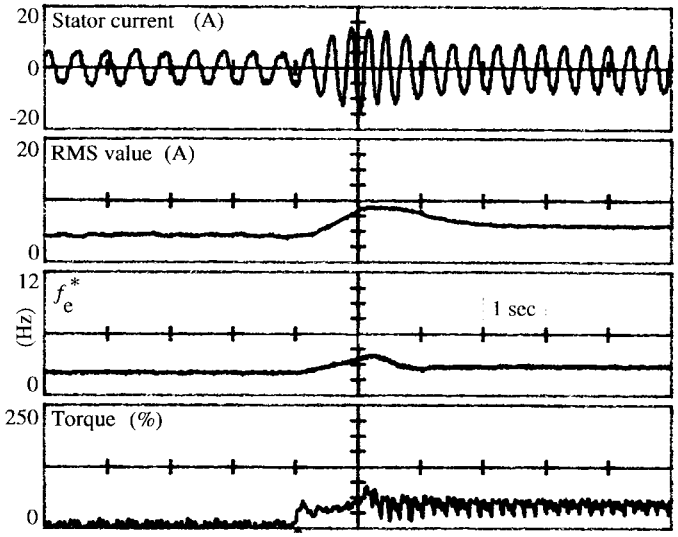

Fig. 15. Experimental rated torque change. Commanded frequency 2 Hz. Speed error 3 r/min. From top: stator current, rms current, commanded frequency, and torque.

The actual voltage and current waveforms obtained in the experimental setup are shown in Fig. 17. From top to bottom, the traces in this figure are phase current, commanded voltage, and measuring flag. The measurement is carried out when the flag is high. From this figure, the need to wait for the transient response to die out before carrying out the measurement is clear.

VII. Inverter Nonlinearity

Since an accurate voltage control is essential to accomplish low-frequency operation and, as mentioned earlier, an accurate

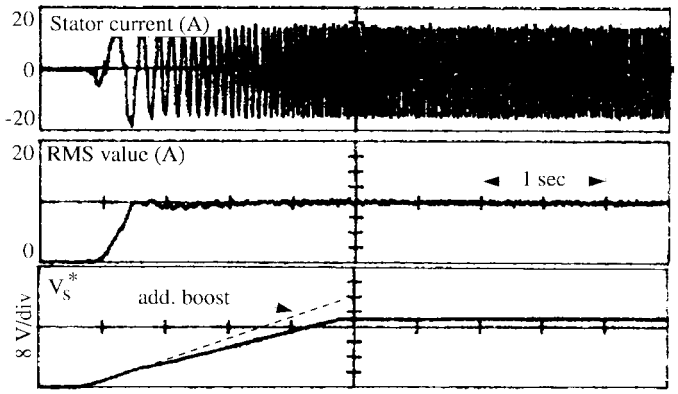

Fig. 16. Experimental acceleration from 0 to 30 Hz. From top: stator current, rms current, and commanded voltage (magnitude).

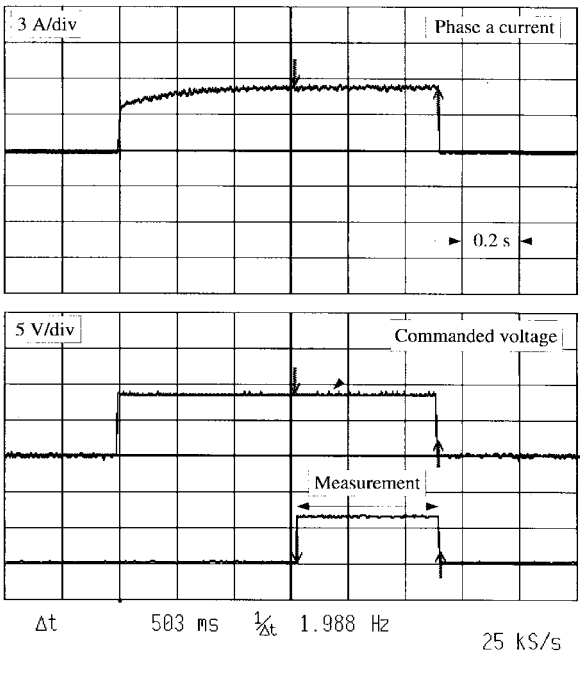

Fig. 17. Stator resistance measurement. From top: phase-a current, phase-a commanded voltage, and measurement flag (high means data acquisition).

synthesis of a reduced output voltage is limited by the nonlinear behavior of a PWM-VSI [8]–[10, [19], it is necessary to provide some means of compensation. The main effects that need to be compensated for are the dead time and the voltage drop across the switches. A detailed discussion of the compensation scheme used goes beyond the scope of this paper and will be presented in a future publication. However, it is important to mention that, in order to achieve a precise speed control in the low-frequency region, a voltage accuracy better than 1 V is required. It is also important to point out that, since the actual blanking time varies with a device's temperature and current, the resulting variation in turn-on and turnoff delays requires that the dead-time compensation must be implemented on-line.

VIII. Conclusions

A new open-loop constant V/f control method has been presented. The influence of the slip regulation, too often neglected, has been studied in detail, and a new compensation method requiring knowledge of only the stator resistance has been proposed. The only measurement needed is the stator current, which is accomplished using a low-cost open-loop type of current transducer. Experimental and simulation results validate the effectiveness of the method and show that good open-loop speed regulation can be achieved. The proposed drive can be easily implemented in existing V/f drives by modifying only the software. Since the only machine parameter needed for the control algorithm is the stator resistance, which is measured during startup using the same PWM inverter and control microprocessor, the system is well suited for operation with off-the-shelf motors, without needing a retuning of the control loops if the motor is replaced. Thus, the proposed drive also exhibits self-commissioning capability.

References

[1] P. L. Alger, *Induction Machines*, 2nd ed. New York: Gordon and Breach, 1970.

[2] R. A. Hamilton and G. R. Lezan, "Thyristor adjustable frequency power supplies for hot strip mill run-out tables," *IEEE Trans. Ind. Gen. Applicat.*, vol. IGA-3, pp. 168–175, Mar./Apr. 1967.

[3] W. Slabiak and L. Lawson, "Precise control of a three-phase squirrel-cage induction motor using a practical cyclconverter," *IEEE Trans. Ind. Gen. Applicat.*, vol. IGA-2, pp. 274–280, July/Aug. 1966.

[4] W. Shepherd and J. Stanway, "An experimental closed-loop variable speed drive incorporating a thyristor driven induction motor," *IEEE Trans. Ind. Gen. Applicat.*, vol. IGA-3, pp. 559–565, Nov./Dec. 1967.

[5] B. K. Bose, Ed., *Power Electronics and Variable Frequency Drives*. New York: IEEE Press, 1996.

[6] F. Blaschke, 'The principle of field orientation as applied to the new transvektor closed-loop control system for rotating-field machines," *Siemens Rev.*, vol. 34, pp. 217–220, 1972.

[7] A. Abbondanti, "Method of flux control in induction motors driven by variable frequency, variable voltage supplies," in *Proc. IEEE-IAS Int. Semi-Annual Power Conversion Conf.*, 1977, pp. 177–184.

[8] Y. Murai, T. Watanabe, and H. Iwasaki, "Waveform distortion and correction circuit for PWM inverters with switching lag-times," *IEEE Trans. Ind. Applicat.*, vol. IA-23, pp. 881–886, Sept./Oct. 1987.

[9] J. W. Choi, S. I. Yong, and S. K. Sul, "Inverter output voltage synthesis using novel dead time compensation," *IEEE Trans. Ind. Applicat.*, vol. 31, pp. 1001–1008, Sept./Oct. 1995.

[10] R. Sepe and J. Lang, "Inverter nonlinearities and discrete-time vector current control," *IEEE Trans. Ind. Applicat.*, vol. 30, pp. 62–70, Jan./Feb. 1994.

[11] K. Koga, R. Ueda, and T. Sonoda, "Achievement of high performances for general purpose inverter drive induction motor system," in *Conf. Rec. IEEE-IAS Annu. Meeting*, 1989, pp. 415–425.

[12] F. A. Stich, "Transistor inverter motor drive having voltage boost at low speeds," U.S. Patent 3 971 972, 1976.

[13] A. Abbondanti, "Flux control system for controlled induction motors," U.S. Patent 3 909 687, 1975.

[14] T. C. Green and B. W. Williams, "Control of induction motor using phase current feedback derived from the DC link," in *Proc. EPE'89*, 1989, vol. III, pp. 1391–1396.

[15] Y. Xue, X. Xu, T. G. Habetler, and D. M. Divan, "A low cost stator oriented voltage source variable speed drive," in *Conf. Rec. IEEE-IAS Annu. Meeting*, 1990, pp. 410–415.

[16] K. Koga, R. Ueda, and T. Sonoda, "Constitution of V/f control for reducing the steady state speed error to zero in induction motor drive system," in *Conf. Rec. IEEE-IAS Annu. Meeting*, 1990, pp. 639–646.

[17] D. W. Novotny and T. A. Lipo, *Vector Control and Dynamics of AC Drives*. Oxford, U.K.: Clarendon, 1996.

[18] S. Nishikata and D. W. Novotny, "Efficiency considerations for low frequency operation of induction motors," in *Conf. Rec. IEEE-IAS Annu. Meeting*, 1988, pp. 91–96.

[19] J. Lee, T. Takeshita, and N. Matsui, "Optimized stator flux oriented sensorless drives of IM in low-speed performance," in *Conf. Rec. IEEE-IAS Annu. Meeting*, 1996, pp. 250–256.

Alfredo Muñoz-García was born in Valparaíso, Chile. He received the B.S. degree in electrical engineering in 1981 from the Technical University Santa Maria, Valparaíso, Chile, and the M.S. degree in electrical engineering in 1995 from the University of Wisconsin, Madison, where he is currently working towards the Ph.D. degree.

From 1981 to 1986, he was with Schlumberger Overseas. In 1987, he became a full-time Lecturer at the Technical University Santa Maria, from where he is currently on leave as a Research Assistant at the University of Wisconsin. He has been involved in several research projects in the areas of variable-frequency drives and power electronics. He was a Fulbright Fellow from 1993 to 1995. His main research interests include electric machines, ac drives, and power electronics.

Thomas A. Lipo (M'64–SM'71–F'87) is a native of Milwaukee, WI.

From 1969 to 1979, he was an Electrical Engineer in the Power Electronics Laboratory, Corporate Research and Development, General Electric Company, Schenectady NY. He became a Professor of Electrical Engineering at Purdue University, West Lafayette, IN, in 1979 and, in 1981, he joined the University of Wisconsin, Madison, in the same capacity, where he is presently the W. W. Grainger Professor for Power Electronics and Electrical Machines.

Dr. Lipo has received the Outstanding Achievement Award from the IEEE Industry Applications Society, the William E. Newell Award of the IEEE Power Electronics Society, and the 1995 Nicola Tesla IEEE Field Award from the IEEE Power Engineering Society for his work. Over the past 30 years, he has served the IEEE in numerous capacities, including President of the IEEE Industry Applications Society.

Donald W. Novotny (M'62–SM'77–F'87) received the B.S. and M.S. degrees in electrical engineering from the Illinois Institute of Technology, Chicago, and the Ph.D. degree from the University of Wisconsin, Madison, in 1956, 1957, and 1961, respectively.

Since 1961, he has been a member of the faculty at the University of Wisconsin, Madison, where he is currently an Emeritus Professor. Prior to retirement in 1996, he was Grainger Professor of Power Electronics and Co-Director of the Wisconsin Electric Machines and Power Consortium (WEMPEC), an educational and research support organization with over 50 industry sponsors. He served as Chairman of the Electrical and Computer Engineering Department from 1976 to 1980 and as an Associate Director of the University–Industry Research Program from 1972 to 1974 and from 1980 to 1993. He has been active as a Consultant to many organizations and has also been a Visiting Professor at Montana State University, the Technical University of Eindhoven, Eindhoven, The Netherlands, the Catholic University of Leuven, Leuven, Belgium, and a Fulbright Lecturer at the University of Ghent, Ghent, Belgium. He has published more than 100 technical articles on electric machines, variable-frequency drives, and power electronic control of industrial systems.

Dr. Novotny is a member of the American Society of Engineering Education, Sigma Xi, Eta Kappa Nu, and Tau Beta Pi and is a Registered Professional Engineer in Wisconsin. He is the recipient of nine Prize Paper Awards from the IEEE Industry Applications Society.